# Nonsymmorphic symmetry and field-driven odd-parity pairing in math xmlns="http://www.w3.org/1998/Math/MathML">mrow>mi>Ce/mi>msub>mi>Rh/mi>mn>2/mn>/msub>msub>mi>As/mi>mn>2/mn>/msub>/mrow>/math>

D. C. Cavanagh, T. Shishidou, M. Weinert, P. M. R. Brydon, and Daniel F. Agterberg

Phys. Rev. B **105**, L020505 — Published 24 January 2022

DOI: 10.1103/PhysRevB.105.L020505

# Non-symmorphic symmetry and field-driven odd-parity pairing in $CeRh_2As_2$

D. C. Cavanagh,[1] T. Shishidou,[2] M. Weinert,[2] P. M. R. Brydon,[3,*] and Daniel F. Agterberg[2,†]

[1] *Department of Physics, University of Otago, P.O. Box 56, Dunedin 9054, New Zealand*
[2] *Department of Physics, University of Wisconsin, Milwaukee, Wisconsin 53201, USA*
[3] *Department of Physics and MacDiarmid Institute for Advanced Materials and Nanotechnology, University of Otago, P.O. Box 56, Dunedin 9054, New Zealand*

Recently, evidence has emerged for a field-induced even- to odd-parity superconducting phase transition in $CeRh_2As_2$ [S. Khim *et al.*, Science **373** 1012 (2021)]. Here we argue that the P4/nmm non-symmorphic crystal structure of $CeRh_2As_2$ plays a key role in enabling this transition by ensuring large spin-orbit interactions near the Brillouin zone boundaries, which naturally leads to the required near-degeneracy of the even- and odd-parity channels. We further comment on the relevance of our theory to FeSe, which crystallizes in the same structure.

*Introduction*—The discovery of a transition between two distinct superconducting phases at high magnetic fields in $CeRh_2As_2$ [1] has generated great interest [2–6]. Due to the immense upper critical field, this has been widely interpreted as a transition between even- and odd-parity pairing states. Creating odd-parity superconductors is a central goal of quantum materials science as they can host non-trivial topological phenomena [7]. The putative field-induced transition in $CeRh_2As_2$ offers a straightforward route to a bulk odd-parity state. As such, it is of great importance to clarify the physics responsible for its remarkable phase diagram.

The even to odd parity transition is enabled by a Rashba-like spin-orbit coupling (SOC) that exists on an inversion ($I$) symmetry breaking sublattice of atoms. $I$ symmetry transforms one sublattice to the other, with opposite signs for SOC, ensuring the Hamiltonian satisfies a global $I$ symmetry. However, the even to odd parity transition is also suppressed by hopping between the two sublattices, and so the SOC should be larger than this inter-sublattice hopping for this transition to occur. It is unclear if this condition can be realized in bulk crystals: Indeed, a relatively strong Rashba-like spin texture has been observed in bilayer cuprate Bi2212 [8], but there is no evidence of a field-induced odd-parity state. Since superconductors with this sublattice structure are not uncommon, the rarity of the field-induced transition suggests that additional physics is necessary to explain the phase diagram of $CeRh_2As_2$.

Here we show that the non-symmorphic (NS) structure of $CeRh_2As_2$ allows the Rashba-like SOC to be larger than the inter-sublattice hopping, providing an explanation for why this transition is observed. In particular, we show that the NS structure ensures that the SOC energy scale is asymptotically larger than that of the inter-sublattice hopping near the Brillouin zone edges. Provided that a Fermi surface with sufficiently large density of states (DOS) exists near the zone edge, the field-induced even- to odd-parity transition can appear at the relatively high temperature seen in $CeRh_2As_2$.

The manuscript is organized as follows: First a general argument is given that on the Brillouin zone edge arbitrary superpositions of Kramers degenerate states have the same spin polarization direction, in contrast to Kramers degenerate states at the Brillouin zone center. This remarkable feature reflects the dominance of SOC near the zone edges. We confirm this by examining a $\boldsymbol{k}\cdot\boldsymbol{p}$ theory valid near the zone edge and contrasting it with one valid near the zone center. This explicitly reveals that the SOC is asymptotically smaller than the inter-sublattice hopping near the zone center, but is asymptotically larger near the zone edge. Considering superconductivity originating from an intra-sublattice pairing instability, the dominance of the SOC at the zone edge allows us to qualitatively reproduce the magnetic field-temperature phase diagram of $CeRh_2As_2$, provided that the contribution to the DOS from the Fermi surfaces near the zone edges is sufficiently large. Density functional calculations for $CeRh_2As_2$ reveal that this can be the case if electron correlations are included. Finally, since our analysis shows that exotic physics due to strong SOC can be expected generically in NS superconductors, we discuss an application of our theory to NS FeSe.

*Non-symmorphic symmetry and spin texture*— In contrast to Kramers degenerate band states at the Brillouin zone center, the NS structure of $CeRh_2As_2$ implies that the two-fold Kramers degenerate band states at the zone edge exhibit the same spin polarization direction. To show this, we consider the set of symmetries that keep momenta lying in the zone-center plane $\boldsymbol{k}_c = (0, k_y, k_z)$ and the zone-edge plane $\boldsymbol{k}_e = (\pi, k_y, k_z)$ unchanged. These include: $M_x$, a mirror reflection through the $\hat{x}$ direction; $T\tilde{I}$, where $T$ is time-reversal symmetry and $\tilde{I} = \{I|\frac{1}{2}, \frac{1}{2}, 0\}$; and their product $T\tilde{I}M_x$. Since $(T\tilde{I})^2 = -1$, these states exhibit a two-fold Kramers degeneracy denoted as $|\boldsymbol{k}_{\nu=e,c}, \pm\rangle \equiv |\nu, \pm\rangle$. These two-fold degenerate eigenstates are also eigenstates of $M_x$, and since $M_x^2 = -1$, $M_x|\nu,\pm\rangle = e_{\nu,\pm}|\nu,\pm\rangle$ where the $e_{\nu,\pm}$ are purely imaginary. From the non-symmorphicity and the general result that $T$ commutes with spatial symmetries, we find $T\tilde{I}M_x = \{E|100\}M_xT\tilde{I}$, where $\{E|100\}$ is an in-plane translation vector. Importantly, $\{E|100\}$ becomes

* philip.brydon@otago.ac.nz
† agterber@uwm.edu

1 for $k_x = 0$, and $-1$ for $k_x = \pi$. Hence, for the zone center plane $M_x(T\tilde{I}|c,\pm\rangle) = -e_{c,\pm}(T\tilde{I}|c,\pm\rangle)$, while for the zone-edge plane $M_x(T\tilde{I}|e,\pm\rangle) = e_{e,\pm}(T\tilde{I}|e,\pm\rangle)$. We thus conclude that Kramers degenerate partners at the zone center plane have *opposite* eigenvalues with respect to $M_x$, while those at the zone boundary have the *same* eigenvalue with respect to $M_x$.

Since the spin operators $S_y$ and $S_z$ are odd under $M_x$, they will have non-zero matrix elements at the zone-center plane, but all their matrix elements are zero at the zone-edge plane [9]. That is, at the zone edges, all eigenstates have their spins polarized along the $\pm\hat{x}$ direction. A similar argument can be made for the $\boldsymbol{k} = (k_x, \pi, k_z)$ plane, where we find that the states are polarized along the $\pm\hat{y}$ direction. This implies that the states in the zone-edge plane cannot couple to a $c$-axis field, while those in the zone center plane can. As seen below, it is this key difference that enhances the $c$-axis Pauli limiting fields and stabilizes a field-induced even- to odd-parity transition for Fermi surfaces near the zone edges relative to those near the zone center.

***k*·*p* *theories*—** To quantify the difference between zone-center and zone-edge Fermi surfaces on superconductivity, we construct $\boldsymbol{k}\cdot\boldsymbol{p}$ theories valid near the Γ point and the M-A Dirac line. (Our results for the M-A Dirac line hold more generally for Fermi surfaces near the zone-edge.) For the Γ point, it suffices to take the small $\boldsymbol{k}$ limit of the tight binding theory presented in Ref. [1]. To develop the $\boldsymbol{k}\cdot\boldsymbol{p}$ theory near the M-A Dirac line [10] we use the representations as given on the Bilbao crystallographic server [11].

In both $\boldsymbol{k}\cdot\boldsymbol{p}$ theories the Hamiltonian has the structure

$$\begin{aligned} H_0 =& \epsilon_{00,\boldsymbol{k}}\tau_0\sigma_0 + \epsilon_{x0,\boldsymbol{k}}\tau_x\sigma_0 + \epsilon_{y0,\boldsymbol{k}}\tau_y\sigma_0 \\ &+ \epsilon_{zx,\boldsymbol{k}}\tau_z\sigma_x + \epsilon_{zy,\boldsymbol{k}}\tau_z\sigma_y + \epsilon_{zz,\boldsymbol{k}}\tau_z\sigma_z. \end{aligned} \tag{1}$$

The $\tau_i$ Pauli matrices encode the sublattice basis composed of two states that are transformed into each other under inversion (e.g., a Ce site basis). The $\sigma_i$ Pauli matrices encode the spin basis. The first line of Eq. (1) describes spin-independent intra- and inter-subllatice hopping processes, whereas the second line includes the SOC terms. $I$ symmetry is given by the operator $\tau_x\sigma_0$ at the Γ, M, and A points. Consequently, $\epsilon_{00,\boldsymbol{k}}$ and $\epsilon_{x0,\boldsymbol{k}}$ are even in momentum $\boldsymbol{k}$, while the other coefficients are odd. Eq. (1) has the same form as a minimal Hamiltonian for a locally non-centrosymmetric material [12–16]. The Hamiltonian possesses two doubly-degenerate eigenvalues $\epsilon_{00,\boldsymbol{k}} \pm \tilde{\epsilon}_{\boldsymbol{k}}$ where

$$\tilde{\epsilon}_{\boldsymbol{k}} = \sqrt{\epsilon^2_{x0,\boldsymbol{k}} + \epsilon^2_{y0,\boldsymbol{k}} + \epsilon^2_{zx,\boldsymbol{k}} + \epsilon^2_{zy,\boldsymbol{k}} + \epsilon^2_{zz,\boldsymbol{k}}}. \tag{2}$$

It is convenient to label the two degenerate states in each band by a pseudospin index. Our choice of pseudospin basis is presented in the SM [17].

In Table I we give the momentum dependence of the coefficients $\epsilon_{\mu\nu,\boldsymbol{k}}$. Along the M-A line we expand radially from the line, i.e., $\boldsymbol{k} = (\pi, \pi, k_z) + (k_x, k_y, 0)$ and expand in $k_x$ and $k_y$. We do not give the form of $\epsilon_{00,\boldsymbol{k}}$ since this term does not play an essential role in the physics, and also only keep the lowest non-zero power of $k_\nu$ in the coefficient of each $\tau_i\sigma_j$ matrix. The $\boldsymbol{k}\cdot\boldsymbol{p}$ theories reveal several remarkable features of the electronic structure: i) The $\epsilon_{zz,\boldsymbol{k}}$ SOC is parametrically smaller than the Rashba-like SOC terms $\epsilon_{zx,\boldsymbol{k}}$ and $\epsilon_{zy,\boldsymbol{k}}$ (and will henceforth be ignored); ii) Near the M-A Dirac line when $k_x = 0$, only the coefficient of $\tau_z\sigma_x$ is non-zero, a consequence of the NS spin texture presented above; iii) The NS symmetry requires that all coefficients vanish at the M-A Dirac line, and hence the energy bands are four-fold degenerate here.

Importantly, the Rashba SOC terms vanish asymptotically more slowly than the inter-sublattice hopping as the M-A Dirac line is approached. This is reflected in the divergence of the ratio $\tilde{\alpha}_{\boldsymbol{k}} = \sqrt{(\epsilon^2_{zx,\boldsymbol{k}} + \epsilon^2_{zy,\boldsymbol{k}})/(\epsilon^2_{x0,\boldsymbol{k}} + \epsilon^2_{y0,\boldsymbol{k}})}$ as one approaches the Dirac line. In contrast, only the inter-sublattice hopping $\epsilon_{x0,\boldsymbol{k}}$ can be nonzero at the Γ point, which implies that the ratio $\tilde{\alpha}_{\boldsymbol{k}}$ vanishes at the zone center. As we shall see, $\tilde{\alpha}_{\boldsymbol{k}}$ plays a key role in our theory.

*Zeeman response*—We include a Zeeman field by adding the term $H_Z = g\mu_B\tau_0\vec{\sigma}\cdot\vec{H}$ to the Hamiltonian Eq. (1). Expressed in the band-pseudospin basis, $H_Z$ typically has both interband and intraband components. The former are not important in the $\tilde{\epsilon}_{\boldsymbol{k}} \gg g\mu|\vec{H}|$ limit; in contrast, the latter lifts the pseudospin degeneracy, acting like an effective pseudospin Zeeman field, which we obtain by projecting $\tau_0\vec{\sigma}$ onto the pseudospin basis, $\tau_0\sigma_\mu \to \vec{\gamma}^\mu_{\boldsymbol{k}}\cdot\vec{s}$. For our choice of pseudospin basis, Zeeman fields parallel (perpendicular) to the $c$-axis produce pseudospin fields that are also parallel (perpendicular) to the $c$-axis; explicit expressions for the effective $g$-factors $\vec{\gamma}^\mu_{\boldsymbol{k}}$ are given in the SM [17]. Moreover, the magnitude of $\vec{\gamma}^\mu_{\boldsymbol{k}}$ is basis-independent and given by

$$|\vec{\gamma}^\mu_{\boldsymbol{k}}|^2 = \hat{\epsilon}^2_{x0,\boldsymbol{k}} + \hat{\epsilon}^2_{y0,\boldsymbol{k}} + \hat{\epsilon}^2_{z\mu,\boldsymbol{k}} \tag{3}$$

where $\hat{\epsilon}_{\mu\nu,\boldsymbol{k}} = \epsilon_{\mu\nu,\boldsymbol{k}}/\tilde{\epsilon}_{\boldsymbol{k}}$. For a $c$-axis field, the pseudospin splitting is controlled by the ratio $\tilde{\alpha}_{\boldsymbol{k}}$ as $|\vec{\gamma}^z_{\boldsymbol{k}}| = (1+\tilde{\alpha}^2_{\boldsymbol{k}})^{-1/2}$. Our $\boldsymbol{k}\cdot\boldsymbol{p}$ theory therefore shows that the pseudospin splitting is maximal near the Γ point, but vanishes as we approach the M-A Dirac line. This reflects the in-plane spin polarization of the band states near the zone edge required by the NS symmetry as discussed above, and implies that the effective $g$-factor vanishes on the zone boundary ($|\vec{\gamma}^z_{\boldsymbol{k}}| = 0$).

*Superconductivity*—In the standard scenario for the field-induced transition in locally $I$-symmetry broken superconductors [18–21], the dominant interaction pairs electrons on the same sublattice in a spin singlet. Since the sublattices are swapped by $I$, this generates both even- and odd-parity states, corresponding to equal and opposite signs of the pairing potential on each sublattice, respectively. We refer to these two possibilities as the uniform and staggered states. The sign difference can be readily encoded in the $\tau$-dependence of the pairing potential, which for the uniform (staggered) state is

| | Γ point | M-A Dirac line |
|---|---|---|
| $\epsilon_{x0,\boldsymbol{k}}$ | $g_{x0}$ | $m^{(e)}_{x0}k_xk_y$ |
| $\epsilon_{y0,\boldsymbol{k}}$ | $g_{y0}k_z$ | $m^{(o)}_{y0}k_xk_y$ |
| $\epsilon_{zx,\boldsymbol{k}}$ | $g_{zx}k_y$ | $m^{(e)}_{zx}k_y$ |
| $\epsilon_{zy,\boldsymbol{k}}$ | $-g_{zx}k_x$ | $-m^{(e)}_{zx}k_x$ |
| $\epsilon_{zz,\boldsymbol{k}}$ | $g_{zz}k_zk_xk_y(k_x^2-k_y^2)$ | $m^{(o)}_{zz}k_xk_y(k_x^2-k_y^2)$ |
| $\tilde{\alpha}^2_{\boldsymbol{k}}$ | $\frac{g^2_{xz}(k_x^2+k_y^2)}{g^2_{x0}} \to 0$ | $\frac{m^{(e)2}_{zx}(k_x^2+k_y^2)}{(m^{(e)2}_{x0}+m^{(o)2}_{y0})k_x^2k_y^2} \to \infty$ |

TABLE I. Form of the nontrivial terms in Eq. (1) near the Γ point and along the M-A Dirac line. The expansion coefficients $m^{(e)}_{ij}$ are functions of $k_z$, with the $(e)$ and $(o)$ superscripts indicating that these are non-vanishing or vanishing at the $M$ and $A$ points. The last row gives $\tilde{\alpha}^2_{\boldsymbol{k}}$, characterizing the ratio of the SOC to the inter-sublattice hopping, and the limiting values as $\boldsymbol{k} \to 0$.

$f_{\boldsymbol{k}}\Delta\tau_0 i\sigma_y$ ($f_{\boldsymbol{k}}\Delta\tau_z i\sigma_y$), where $f_{\boldsymbol{k}}$ is an even-parity form factor.

In the pseudospin basis, the uniform and staggered pairing potentials are

$$\Delta f_{\boldsymbol{k}}\tau_0 i\sigma_y \to \Delta f_{\boldsymbol{k}} i s_y \tag{4}$$

$$\Delta f_{\boldsymbol{k}}\tau_z i\sigma_y \to \pm\left(\hat{\epsilon}_{zx,\boldsymbol{k}}s_x + \hat{\epsilon}_{zy,\boldsymbol{k}}s_y\right)\Delta f_{\boldsymbol{k}} i s_y\,. \tag{5}$$

The odd-parity staggered state is transformed into a helical pseudospin-triplet state, with reduced gap magnitude $\sqrt{\hat{\epsilon}^2_{zx,\boldsymbol{k}}+\hat{\epsilon}^2_{zy,\boldsymbol{k}}}|\Delta f_{\boldsymbol{k}}|$ and opposite sign in each band. The reduced gap magnitude of the staggered state is due to interband pairing, implying that this state has a lower transition temperature ($T_c$) than the uniform state. In the weak-coupling limit the $T_c$ of the staggered state is determined by an effective coupling constant which is smaller than that of the uniform state by $\langle\hat{\epsilon}^2_{zx,\boldsymbol{k}}+\hat{\epsilon}^2_{zy,\boldsymbol{k}}\rangle_{\rm FS} = \langle\tilde{\alpha}^2_{\boldsymbol{k}}/(1+\tilde{\alpha}^2_{\boldsymbol{k}})\rangle_{\rm FS}$ where the average is taken over the Fermi surface [22]. Due to the exponential sensitivity of $T_c$ on the coupling constant, the ratio $\tilde{\alpha}_{\boldsymbol{k}}$ must be larger than unity for $T_c$ of the staggered and uniform states to be comparable.

The projection onto the pseudospin basis reveals the essential physics of the field-induced transition. Since the same interaction mediates pairing in both channels, the generically smaller gap opened by the staggered state implies that it has the lower $T_c$ at zero field. However, whereas the uniform state is Pauli limited (albeit with an enhanced upper critical field due to the reduced effective $g$ factor [15]), the staggered state is not Pauli limited for a $c$-axis field, since the effective pseudospin Zeeman field is perpendicular to the $\vec{d}$-vector of the pseudospin triplet state. Thus, a field-induced transition occurs when a $c$-axis field suppresses the uniform state below the $T_c$ of the staggered state.

The key parameter that underlies both the $T_c$ of the staggered state and the response of the uniform state to $c$-axis fields is $\tilde{\alpha}_{\boldsymbol{k}}$. Crucially, our $\boldsymbol{k}\cdot\boldsymbol{p}$ analysis shows that $\tilde{\alpha}_{\boldsymbol{k}}$ strongly varies across the Brillouin zone in $CeRh_2As_2$ due to the NS crystal symmetry. In particular, although

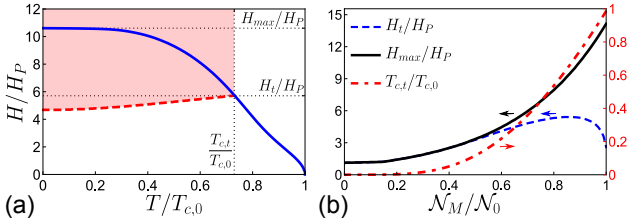


FIG. 1. (a) Phase diagram for $\mathcal{N}_M = 0.9\mathcal{N}_0$: the blue line gives the upper critical field of the uniform state, and the red dashed line gives the boundary of the staggered state. The staggered state is realized in the shaded region. (b) The dependence of the upper critical field of the uniform state ($H_{\rm max}$, black solid line) and the critical field ($H_t$, blue dashed line) and temperature ($T_{c,t}$ red dot-dashed line) at which the field-induced transition occurs as a function of the contribution of the density of states at the M point to the total density of states. The field strengths are expressed in terms of the Pauli limiting field $H_P \approx 1.25 k_B T_{c,0}$.

it vanishes upon approaching the Γ point, $\tilde{\alpha}_{\boldsymbol{k}}$ diverges towards the M-A Dirac line due to the vanishing inter-sublattice terms, as indicated in Table I. Remarkably, the NS symmetry-enforced spin polarization of the band states at the Brillouin zone edge implies that $\tilde{\alpha}_R$ *diverges on these planes*. Thus, large values of $\tilde{\alpha}_{\boldsymbol{k}}$ are generically expected for Fermi surfaces sufficiently near the zone edge. In $CeRh_2As_2$, the field-induced transition occurs at $T_{c,t} \approx 0.7T_{c,0}$, where $T_{c,0}$ is the zero-field transition temperature, implying that $\tilde{\alpha}_{\boldsymbol{k}} \approx 3.5$ at the Fermi energy. Our theory shows that such ratios are possible if states near the Brillouin zone edge make a significant contribution to the DOS at the Fermi energy. Previous theoretical studies of $CeRh_2As_2$ have assumed Fermi surfaces near the Γ point, where the enhancement of $\tilde{\alpha}_{\boldsymbol{k}}$ due to the NS symmetry is not apparent [4–6]; as in similar treatments of symmorphic lattices [18–21], these theories require an unexpectedly large SOC strength to explain the field-induced transition.

It is instructive to contrast our results with previous results in $I$-symmetric 2D Ising superconductors [23–25] and a toy model of a 1D NS zig-zag chain [26]. In the Ising systems, a symmetry-required divergence of the ratio $\tilde{\alpha}_{\boldsymbol{k}}$ occurs for band representations with angular momentum $j_z = \pm 3/2$ at certain points in the 2D Brillouin zone, which strongly enhances the Pauli limit field for in-plane fields. Our result is more general, however, as the divergent $\tilde{\alpha}_{\boldsymbol{k}}$ occurs on a 2D manifold of the 3D Brillouin zone, and holds for all band representations. In the zig-zag chain, the stability of an odd-parity state similar to that discussed here is found to be enhanced when the 1D FS is near the zone edge [26]. Although the corresponding ratio $\tilde{\alpha}_k$ does take a maximum at the zone-edge, it does not diverge as in our model. Consequently, the NS spin texture mechanism we examine is a more general route to enhancing the effect of SOC.

*Two-pocket model*—While Fermi surfaces near the zone edge favor a field-induced transition, it is likely that they

will appear together with other Fermi surfaces near the zone center where the parameter $\tilde{\alpha}_{\boldsymbol{k}}$ is small. To examine the sensitivity of our theory to the presence of these additional Fermi surfaces, we consider a model of $CeRh_2As_2$ with two cylindrical Fermi pockets centered on the Γ-Z and M-A Dirac lines, fixing $|\vec{\gamma}^z_{\boldsymbol{k}}| = 0.9$ and $0.1|\hat{k}_x\hat{k}_y|$ on the two Fermi surfaces, corresponding to small and large values of $\tilde{\alpha}_{\boldsymbol{k}}$, respectively. The momentum-dependence of the effective $g$-factor near the M-A Dirac line reflects the NS symmetry-enforced spin texture at the zone boundary. Assuming an intrasublattice pairing interaction, we use standard techniques to construct the field-temperature phase diagram, see the SM for details [17]. For simplicity we assume an $s$-wave form factor, i.e. $f_{\boldsymbol{k}} = 1$, but our results are robust to other choices.

In Fig. 1(a), we present a phase diagram which qualitatively agrees with that observed in $CeRh_2As_2$. Since we only consider the Zeeman effect, the upper critical field of the staggered state is infinite, and so the right-most boundary of the staggered state is vertical; including orbital effects will give a finite upper critical field [2], but does not qualitatively alter our theory. Fig. 1(a) was found by setting the M-A pocket DOS at 90% the total DOS. In Fig. 1(b) we examine the consequences of varying this M-A pocket DOS for the upper critical field of the uniform state, and the field strength and temperature at which the transition into the staggered state occurs. The field-induced transition is strongly enhanced as the contribution of the M-A pocket to the DOS increases, with the even- and odd-parity states near-degenerate when this is the only Fermi surface. Importantly, the field-induced transition occurs at an observable temperature $T_{c,t} > 0.1T_{c0}$ if the M-A pocket makes up at least half of the DOS.

*DFT results*—DFT calculations and analysis were carried out to explore the possibility that the Fermi surface of $CeRh_2As_2$ contains regions near the zone-edge and to verify that the states at the zone-edge exhibit the spin polarization found above. As shown in the SM [17], the Fermi surface (shown in Fig. S1a) predicted by the DFT bands consists of four pockets about the A point that do not intersect the zone edge, and portions about the Γ-Z line, representing ∼53% of the DOS, in agreement with [6]. This Fermi surface is unlikely to be consistent with the observed odd-parity state.

The experimental heat jump at the superconducting transition temperature suggest fermion masses a factor 100-1000 larger than the bare electron mass, implying that the Ce $4f$ electrons are itinerant. The standard DFT results are inconsistent with this enhanced effective mass. To address this, we have employed a renormalized band structure approach similar to that pioneered by Zwicknagl [27, 28]. Fig. 2a shows the resulting band structure; the corresponding Fermi surface, Fig. 2b, has a DOS 10 times larger than standard DFT and agrees with that found in Ref. [29]. Moreover, the pockets at the zone boundary account for 80% of the total DOS, consistent

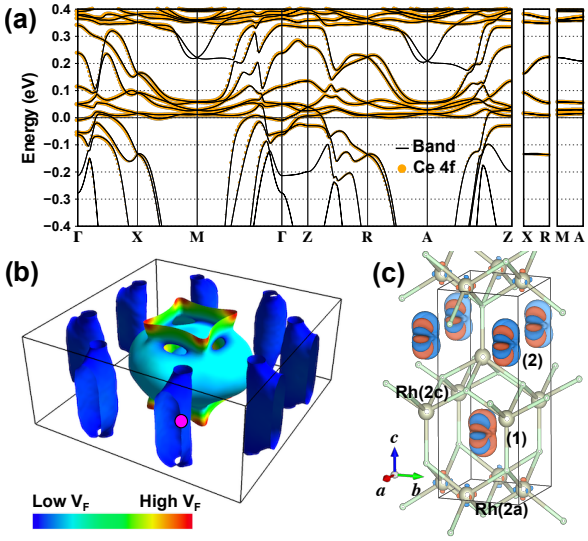


FIG. 2. (a) Bands including $4f$ electron correlations through a renormalized band structure approach with Ce $4f$ weight represented by orange dots. (b) Fermi surface for (a). (c) $x$-component spin density distribution of the doubly degenerate bands at a point on zone edge marked by the pink circle in (b). Red/blue represents positive/negative spin density.

with the observed odd-parity state. In the SM, we show that with different choices of renormalizations, the DOS can be further increased (with similar Fermi surfaces), and also explore the effects on the band structure from several other scenarios within DFT. Figure 2(c) shows the $S_x$ spin density arising from a Kramers pair on the zone boundary; the integrated spin density around each atom is non-vanishing only for $S_x$ and is opposite on the two sublattices, in agreement with the symmetry-based arguments presented above.

*Discussion and conclusions*—Our key result is that the NS P4/nmm structure of $CeRh_2As_2$ enables the SOC structure required to stabilize an odd-parity superconducting state under field and to enhance the critical field along the $c$-axis. It is natural to ask if there exist other materials with the same structure for which this is also the case. Remarkably, there exist experimental results on superconducting FeSe, also with a P4/nmm structure, that suggest similar considerations apply. In particular, Knight shift measurements indicate that there is no change in the spin susceptibility upon entering the superconducting state for the field applied along the $c$-axis [30, 31]. This could be explained by a nearly-vanishing g-factor for a $c$-axis Zeeman field due to strong SOC. This implies that the Zeeman coupling only produces a van-Vleck-like spin susceptibility which is largely unchanged by superconductivity [18]. In addition, there exists evidence for an unexplained $c$-axis field-induced superconducting phase transition for fields much larger than the Pauli limiting field [32]. The possibility that this transition corresponds to a transition from an even to odd parity phase is currently under investigation.

*Acknowledgements*– MW and TS were supported by the US Department of Energy, Office of Basic Energy Sciences, Division of Materials Sciences and Engineering under Award DE-SC0017632. DCC and PMRB were supported by the Marsden Fund Council from Government funding, managed by Royal Society Te Apārangi. DFA was supported by the US Department of Energy, Office of Basic Energy Sciences, Division of Materials Sciences and Engineering under Award DE-SC0021971. We acknowledge useful discussions with Manuel Brando, Mark Fischer, Christoph Geibel, Elena Hassinger, Seunghyun Khim, Andy Mackenzie, Igor Mazin, and Manfred Sigrist.

[1] S. Khim, J. F. Landaeta, J. Banda, N. Bannor, M. Brando, P. M. R. Brydon, D. Hafner, R. Küchler, R. Cardoso-Gil, U. Stockert, A. P. Mackenzie, D. F. Agterberg, C. Geibel, and E. Hassinger, Science **373**, 1012 (2021).

[2] E. G. Schertenleib, M. H. Fischer, and M. Sigrist, Phys. Rev. Research **3**, 023179 (2021).

[3] A. Ptok, K. J. Kapcia, P. T. Jochym, J. Łażewski, A. M. Oleś, and P. Piekarz, Phys. Rev. B **104**, L041109 (2021).

[4] D. Möckli and A. Ramires, Phys. Rev. Research **3**, 023204 (2021).

[5] A. Skurativska, M. Sigrist, and M. H. Fischer, Phys. Rev. Research **3**, 033133 (2021).

[6] K. Nogaki, A. Daido, J. Ishizuka, and Y. Yanase, "Topological crystalline superconductivity in locally noncentrosymmetric $CeRh_2As_2$," (2021), arXiv:2103.08088 [cond-mat.supr-con].

[7] M. Sato and Y. Ando, Reports on Progress in Physics **80**, 076501 (2017).

[8] K. Gotlieb, C.-Y. Lin, M. Serbyn, W. Zhang, C. L. Smallwood, C. Jozwiak, H. Eisaki, Z. Hussain, A. Vishwanath, and A. Lanzara, Science **362**, 1271 (2018).

[9] A proof is as follows: The matrix elements of the $j$ spin operator with respect to the pseudospin partners are $\langle \nu, m|S_j|\nu, m'\rangle = \langle \nu, m|\tilde{M}_x^{-1}\tilde{M}_x S_j \tilde{M}_x^{-1}\tilde{M}_x|\nu, m'\rangle = e^*_{\nu,m}e_{\nu,m'}(-1)^j\langle \nu, m|S_j|\nu, m'\rangle$, where $(-1)^j = -1$ (1) for $j = z$, $y$ ($x$), and $e_{\nu,m}$ is the eigenvalue of $\tilde{M}_x$. Since the states at the zone boundary have the same eigenvalues, we conclude that all the matrix elements for the $z$ and $y$ spin operators are vanishing.

[10] S. M. Young, S. Zaheer, J. C. Y. Teo, C. L. Kane, E. J. Mele, and A. M. Rappe, Phys. Rev. Lett. **108**, 140405 (2012).

[11] M. I. Aroyo, J. M. Perez-Mato, C. Capillas, E. Kroumova, S. Ivantchev, G. Madariaga, A. Kirov, and H. Wondratschek, Zeitschrift für Kristallographie **221**, 15 (2006); M. I. Aroyo, A. Kirov, C. Capillas, J. M. Perez-Mato, and H. Wondratschek, Acta Crystallographica Section A **62**, 115 (2006).

[12] L. Fu and E. Berg, Phys. Rev. Lett. **105**, 097001 (2010).

[13] S. J. Youn, M. H. Fischer, S. H. Rhim, M. Sigrist, and D. F. Agterberg, Phys. Rev. B **85**, 220505 (2012).

[14] Y. Yanase, Phys. Rev. B **94**, 174502 (2016).

[15] Y.-M. Xie, B. T. Zhou, and K. T. Law, Phys. Rev. Lett. **125**, 107001 (2020).

[16] T. Shishidou, H. G. Suh, P. M. R. Brydon, M. Weinert, and D. F. Agterberg, Phys. Rev. B **103**, 104504 (2021).

[17] See the Supplemental Material at .... for details of the DFT calculations, the pseudospin basis, and the calculation of the phase diagram. This includes Ref.s [33–39].

[18] M. H. Fischer, F. Loder, and M. Sigrist, Phys. Rev. B **84**, 184533 (2011).

[19] T. Yoshida, M. Sigrist, and Y. Yanase, Phys. Rev. B **86**, 134514 (2012).

[20] T. Yoshida, M. Sigrist, and Y. Yanase, Journal of the Physical Society of Japan **83**, 013703 (2014).

[21] M. Sigrist, D. F. Agterberg, M. H. Fischer, J. Goryo, F. Loder, S.-H. Rhim, D. Maruyama, Y. Yanase, T. Yoshida, and S. J. Youn, Journal of the Physical Society of Japan **83**, 061014 (2014).

[22] A. Ramires, D. F. Agterberg, and M. Sigrist, Phys. Rev. B **98**, 024501 (2018).

[23] Y. Nakamura and Y. Yanase, Phys. Rev. B **96**, 054501 (2017).

[24] C. Wang, B. Lian, X. Guo, J. Mao, Z. Zhang, D. Zhang, B.-L. Gu, Y. Xu, and W. Duan, Phys. Rev. Lett. **123**, 126402 (2019).

[25] J. Falson, Y. Xu, M. Liao, Y. Zang, K. Zhu, C. Wang, Z. Zhang, H. Liu, W. Duan, K. He, H. Liu, J. H. Smet, D. Zhang, and Q.-K. Xue, Science **367**, 1454 (2020).

[26] S. Sumita and Y. Yanase, Physical Review B **93** (2016).

[27] G. Zwicknagl, Advances in Physics **41**, 203 (1992).

[28] G. Zwicknagl, Reports on Progress in Physics **79**, 124501 (2016).

[29] D. Hafner, P. Khanenko, E. O. Eljaouhari, R. Kchler, J. Banda, N. Bannor, T. Lhmann, J. F. Landaeta, S. Mishra, I. Sheikin, E. Hassinger, S. Khim, C. Geibel, G. Zwicknagl, and M. Brando, "Possible quadrupole density wave in the superconducting Kondo lattice $CeRh_2As_2$," (2021), arXiv:2108.06267 [cond-mat.str-el].

[30] I. Vinograd, S. P. Edwards, Z. Wang, T. Kissikov, J. K. Byland, J. R. Badger, V. Taufour, and N. J. Curro, Phys. Rev. B **104**, 014502 (2021).

[31] S. Molatta, D. Opherden, J. Wosnitza, L. Opherden, Z. T. Zhang, T. Wolf, H. v. Löhneysen, R. Sarkar, P. K. Biswas, H.-J. Grafe, and H. Kühne, Phys. Rev. B **104**, 014504 (2021).

[32] S. Kasahara, T. Watashige, T. Hanaguri, Y. Kohsaka, T. Yamashita, Y. Shimoyama, Y. Mizukami, R. Endo, H. Ikeda, K. Aoyama, T. Terashima, S. Uji, T. Wolf, H. von Löhneysen, T. Shibauchi, and Y. Matsuda, PNAS **111**, 16309 (2014).

[33] M. Weinert, G. Schneider, R. Podloucky, and J. Redinger, J. Phys. Condens. Matter **21**, 084201 (2009).

[34] J. P. Perdew, K. Burke, and M. Ernzerhof, Phys. Rev. Lett. **77**, 3865 (1996).

[35] M. Kawamura, Computer Physics Communications **239**, 197 (2019).

[36] K. Momma and F. Izumi, Journal of Applied Crystallography **44**, 1272 (2011).

[37] C. M. Varma, Rev. Mod. Phys. **48**, 219 (1976).

[38] G. W. Scheerer, Z. Ren, S. Watanabe, G. Lapertot, D. Aoki, D. Jaccard, and K. Miyake, npj Quantum Materials **3**, 41 (2018).

[39] L. Fu, Phys. Rev. Lett. **115**, 026401 (2015).